Partial Evaporation of Strontium Zirconate During Atmospheric Plasma Spraying

Yanfei Zhang, Daniel Emil Mack, Maria Ophelia Jarligo, Xueqiang Cao, Robert Vaßen, and Detlev Stöver

Perovskite-type $SrZrO_3$ has been investigated as a candidate material for thermal barrier coating application. During plasma spraying of $SrZrO_3$, SrO volatilized more than ZrO_2 and the coating composition deviates from initial stoichiometry. In this investigation, partial evaporation was investigated by spraying $SrZrO_3$ powders into water. The influences of spraying current, distance and particle size of the powder on the partial evaporation were also investigated in a quantitative way. With optimized spraying parameters, stoichiometric $SrZrO_3$ coating was produced by adding an excess amount of Sr in the precursors before plasma spraying to compensate for the volatilized component.

1. Introduction

The use of thermal barrier coatings (TBCs) allows the increase of the turbine inlet temperature, hence an increase of the efficiency of turbine engines (Ref 1, 2). Plasma-sprayed TBCs typically consist of an oxidation-resistant metallic MCrAlY (M = Ni and/or Co) bond coat and a ceramic top coat. Present top coat materials are based on 7-8 wt.% Y_2O_3-stabilized ZrO_2. However, at higher temperature, volume changes induced by phase transformation and sintering give rise to cracks, leading to coating failure. To overcome this shortcoming, the search for new TBCs materials has been intensified. Perovskite-type $SrZrO_3$ has been investigated as candidate TBCs material. Details of $SrZrO_3$ are published in literature (Ref 1, 2), and Table 1 summarizes its thermophysical properties.

Besides electron beam physical vapor deposition, usually TBCs are deposited by atmospheric plasma spraying with typically very high plasma flame temperature. The rapid heating of the particles gives rise to melting of the particles, sublimation, vaporization and evaporation across a liquid-vapor interface. Vaporization is driven by vapor concentration gradients existing between the free stream and the particle surface at temperatures below the boiling point while evaporation happens as the surface temperature reaches the boiling point (Ref 4). Physical vaporization and evaporation of the powders has no component change, which is controlled by vapor diffusion and heat transfer (Ref 5). In addition, plasma spraying can be accompanied by selective evaporation of a component of multi-component powder (Ref 6). As the material is heated in the plasma flame, substantial different evaporation rates of the constituents will lead to stoichiometry changes (Ref 7). For example, partial evaporation of CuO from $YBa_2Cu_3O_x$ (Ref 6), P_2O_5 from $Ca_5(PO_4)_3OH$ (Ref 8), La_2O_3 from $La_2Zr_2O_7$ (Ref 7) and CeO_2 from $La_2Ce_2O_7$ (Ref 9) have been reported.

During plasma spraying of $SrZrO_3$, SrO was found to volatilize faster than ZrO_2 with the result that the coating composition deviated from stoichiometric composition (Ref 2). The existence of excess ZrO_2 in the plasma-sprayed $SrZrO_3$ coating might influence the coating properties. To deposit a stoichiometric $SrZrO_3$ coating, an excess amount of Sr must be added in the precursors before plasma spraying to compensate the loss of SrO by partial evaporation.

Although partial evaporation during plasma spraying of multi-oxides is common, detailed investigation of this phenomenon is very limited. Accurate analysis of evaporation mechanisms involved during plasma spraying of multi-oxides is necessary. This paper presents the quantitative investigation of the partial evaporation of $SrZrO_3$ by spraying powders into water.

Yanfei Zhang, Forschungszentrum Jülich GmbH, IEF-1, 52425 Jülich, Germany; State Key Laboratory of Rare Earth Resources Utilization, Changchun Institute of Applied Chemistry, Chinese Academy of Sciences, Changchun 130022 Jilin, China; and Graduate School of Chinese Academy of Sciences, Beijing 100049, China; **Daniel Emil Mack, Maria Ophelia Jarligo, Robert Vaßen,** and **Detlev Stöver**, Forschungszentrum Jülich GmbH, IEF-1, 52425 Jülich, Germany; and **Xueqiang Cao**, State Key Laboratory of Rare Earth Resources Utilization, Changchun Institute of Applied Chemistry, Chinese Academy of Sciences, Changchun 130022 Jilin, China. Contact e-mail: ya.zhang@fz-juelich.de.

2. Experimental

2.1 Plasma Spraying

Commercial $SrCO_3$ (Aldrich, >98%, Munich, Germany) and ZrO_2 (Aldrich, 99%, Munich, Germany) powders

Table 1 Thermophysical properties of SrZrO₃ (Ref 1-3)

Crystal system	Orthorhombic
Lattice parameters, nm	
a	0.5816
b	0.8225
c	0.5813
Thermal expansion coefficients, K^{-1}	
α	10.9×10^{-6}
Melting point, K	
T_m	2883
Shear modulus, GPa	
G	98.5
Young's modulus	
E	269
Debye temperature, K	
θ_D	591
Vickers hardness, GPa	
Hv	5.74
Thermal conductivity at 1000 °C, $W\cdot(m\cdot K)^{-1}$	
λ	2.08
"Steady state" sintering rate at 1200 °C, s^{-1}	1.04×10^{-9}

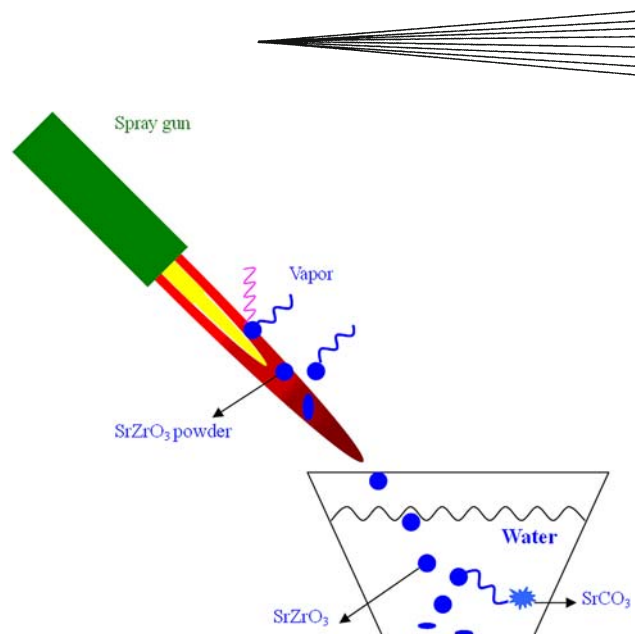**Fig. 1** Schematic illustration of plasma spraying SrZrO₃ into water

were mixed by ball-milling with a Sr/Zr atomic ratio of 1.136 and calcined at 1400 °C for 24 h with a heating rate of 5 K/min. This means more than 10% of Sr was added in the precursors. The powders were spray-dried in a spray-dryer (Mobile MinorTM'2000' Ex Model H) with N_2 as the drying medium, then heat treated at 1300 °C for 5 h to remove the organic binding compounds.

All plasma-sprayed coatings have been produced with a three cathode gun Triplex II in a Multicoat facility produced by Sulzer Metco, Wohlen, Switzerland. The gun was mounted on a 6-axis robot, which allowed well-defined coating sequences. Sand blasted austenitic steel was used as substrate for the coatings. The dimension of the standard steel substrates was a square with a side length of 50 mm and a thickness of 2 mm. Substrate temperatures were measured using the 4 M8 pyrometer system (Land instruments GmbH, Germany). These coatings were sprayed with argon and helium as plasma gases with flow rates of 45 and 6 standard liters per minute (slpm), respectively. The feeding gas was 2 slpm of Ar. The Robert speed was 500 mm/s. Particle speed and temperature monitoring were performed by an Accura spray-g3 diagnostic system (Tecnar, St. Bruno, Canada).

With a Triplex I gun (Sulzer Metco, Wohlen, Switzerland), some SrZrO₃ powders were also sprayed into water to investigate the evaporation of oxide components. The schematic illustration is shown in Fig. 1. The argon and helium plasma gas flow rates during spraying were 20 and 13 slpm, respectively. The feeding gas was 1.5 slpm of Ar. The spraying distance from the exit of the torch and the water was 320 mm and the spraying angle was 45°. A 4L boiler filled with ordinary water was used to collect plasma-sprayed powders. After plasma spraying, the solution was evaporated until totally dry. The collected powders were characterized.

2.2 Characterization

The phase composition of the powders was analyzed by x-ray diffraction (XRD) with a D500 diffractometer

(Siemens AG, Germany) equipped with diffracted-beam monochromator for Cu-Kα. Particle size distribution was measured by Fraunhofer diffraction with 633 nm laser light using the Analysette 22 (Fritsch GmbH, Idar Oberstein, Germany). Chemical analysis of samples was performed using optical emission spectroscopy (OES 4.1, TJAIRIS-INTREPID) after evaporation in inductively coupled plasma (ICP). After plasma treatment, the SrZrO₃ powders were vacuum impregnated with epoxy. After hardening of the resin, the sample was ground mechanically with SiC abrasive paper and polished on soft disks with diamond suspension. A cross section of the sample was investigated by a scanning electron microscope (SEM) (ModelJXA 840, JEOL, Tokyo, Japan) with an energy dispersive x-ray spectrometer (EDX) (Model Inca, Oxford Instruments, Oxfordshire, UK).
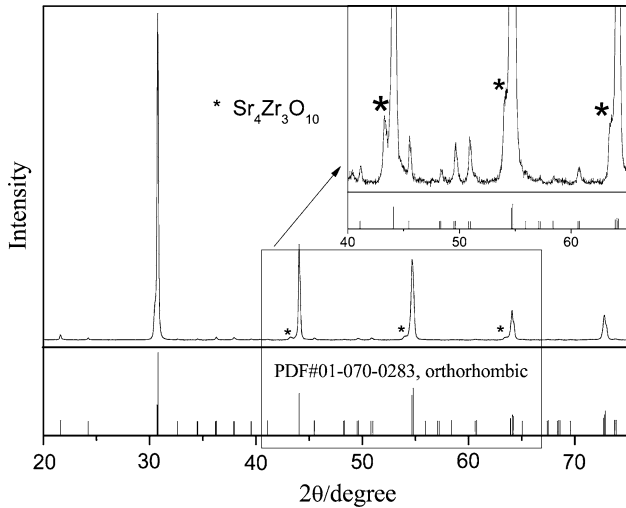
3. Results and Discussion

3.1 Composition of the Synthesized Powders

An excess amount of SrO was added in before calcination and Sr/Zr ratio of this powder is 1.136. The XRD result of the synthesized powders is shown in Fig. 2. The main phase composition was found to be SrZrO₃ (PDF#01-070-0283, Orthorhombic) and the secondary phase was $Sr_4Zr_3O_{10}$ (JCPDS#23-1416, Orthorhombic). This result is in accordance with ZrO_2-SrO phase diagram (Fig. 3). No other phases were detected.

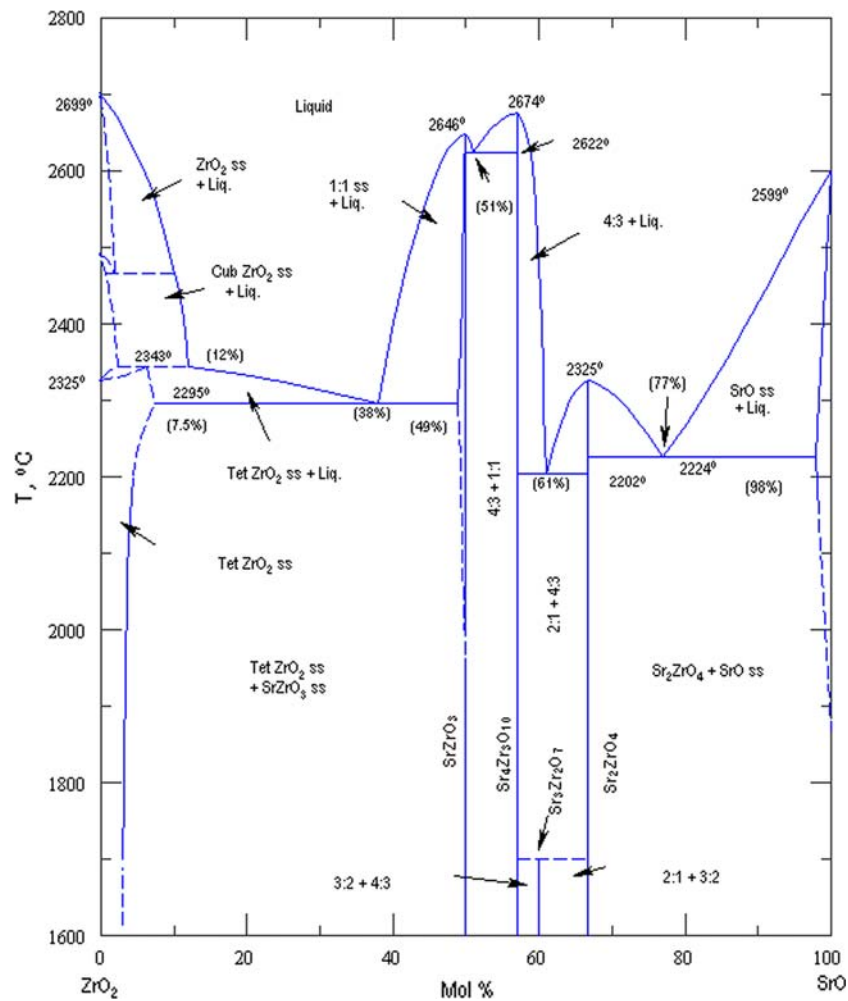### 3.2 Powders Plasma-Sprayed into Water

After spray-drying and before plasma spraying, powders were sintered at 1300 °C for 5 h. Furnace heat treatment of the spray-dried powders has many advantages. Heat treatment will remove the organic binding compounds, make the particles dense and increase the
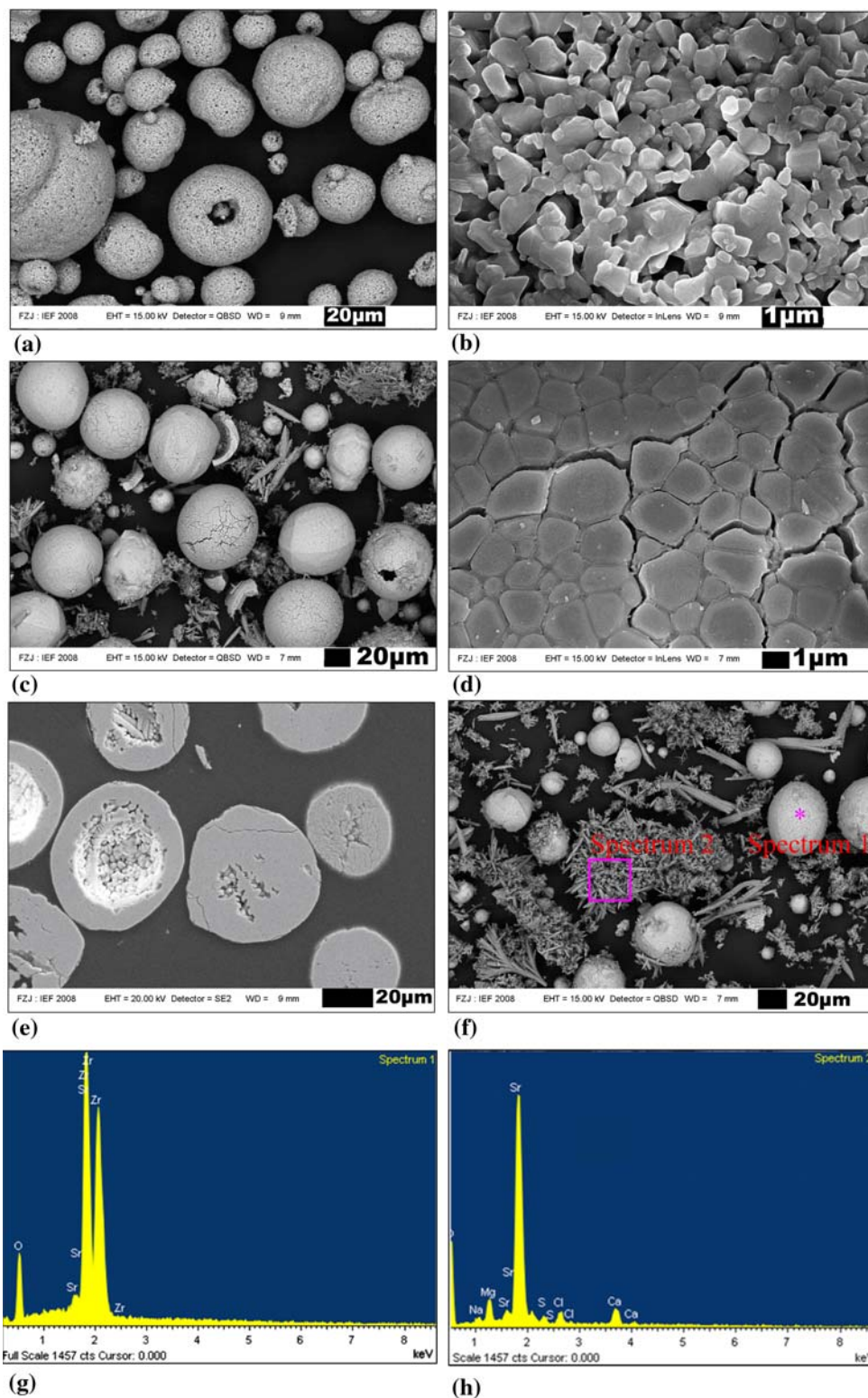
Fig. 2 XRD of SrZrO₃ powders after calcination (1400 °C for 24 h) and before spray-drying

mechanical stability of the powders. Figure 4(a) indicates the morphology of spray-dried powders after being sintered at 1300 °C for 5 h. Most of the spray-dried powders are spherical and some are hollow. During spray-drying the large-sized pores inside the particles result mainly from the evaporation of liquid and the small-sized pores result from the incomplete sintering of the submicron precursors. The surface of the particles is very porous (Fig. 4b). Such a way of obtaining hollow particles can be useful to produce powders resulting in coatings of controlled properties, such as thermal conductivity or elastic modulus (Ref 11). Compared with irregular shape powders, spherical particles have better flowability. During thermal spraying, these spherical and free-flowing powders can enter the center of the plasma flame easily.

Although the processes of plasma spraying of coatings and plasma treatment of powders are very similar, their final products are totally different. The plasma treatment of powders is usually carried out to improve some of their properties, such as flowability, density, internal or external
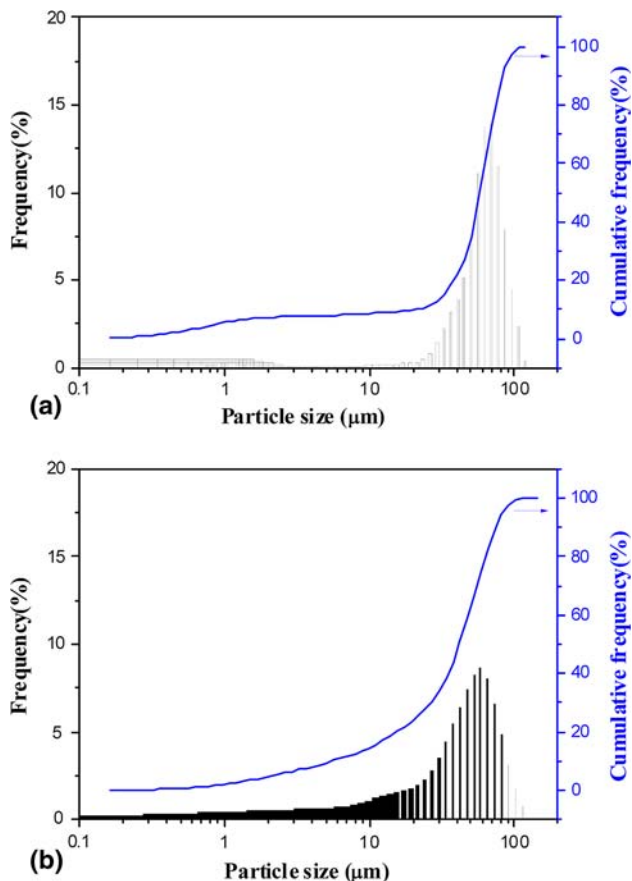

Fig. 3 ZrO₂-SrO phase diagram (Ref 10)

Fig. 4 (a) Spray-dried powders after sintering at 1300 °C; (b) surface of the powders after sintering at 1300 °C; (c) powders plasma-sprayed into water; (d) surface of the powders sprayed into water; (e) cross section of the powders sprayed into water; (f) spherical particles and newly formed needle-like structure; (g) EDX of spherical particles; and (h) EDX of newly formed structure

morphology, etc. (Ref 11). As shown in Fig. 4(c), most of the spherical structures were preserved after plasma treatment. However, some new needle-like structures were formed after plasma treatment. As shown in Fig. 4(d), the surface of the powders became much denser after plasma treatment. Cross section of the powders (Fig. 4e) indicates that most of the spray-dried powders were densified in the plasma flame. Some spheres have a porous center with a dense outer shell. Big holes in the center of powders can be found after being plasma-sprayed into water. As the $SrZrO_3$ powders were prepared by the spray-drying method, particles were initially spherical but very porous. During plasma treatment a large temperature gradient exists between the surface and the core of a porous particle. $SrZrO_3$ has low thermal conductivity and it is possible to have the surface melting, evaporating and the core still remain porous (Ref 12). Therefore, heating, melting and evaporation may proceed at the same time in such a particle (Ref 13).

The particle size distributions of the spray-dried powders before and after being plasma-sprayed into water are shown in Fig. 5(a) and (b), respectively. Both frequency histograms and cumulative frequency curves are indicated with logarithmic abscissa. The maximum frequency decreased from 13 to 8% after plasma-sprayed into water.

Fig. 5 Particle size distributions of spray-dried powders before (a) and after (b) being plasma-sprayed into water

The histogram also became wider and the proportion of lower size particles became higher. These prove distribution of plasma-treated powder size is shifted in the direction of smaller sizes. After plasma processing, usually the distribution of powder sizes shifts in the direction of smaller sizes (Ref 8, 11). The particle size decrease of the powders during plasma treatment is caused by densification and shrinkage because powders are molten totally or partially in the plasma flame. The smallest particles might be blown away or totally evaporated in the plasma flame and only larger particles were preserved.

As shown in Fig. 4(g), after plasma treatment, the composition of the spherical powders is still $SrZrO_3$. However, main composition of the newly formed needle-like structure is Sr and no Zr can be detected in the new structure (Fig. 4h). In spectrum 2 (Fig. 4h), the Ca, Mg, Na, S and Cl are probably from ordinary water used for collecting powders during plasma spraying.

Chemical compositions of the $SrZrO_3$ powders before and after plasma treatment are listed in Table 2. Chemical analysis indicates that before plasma treatment, the Sr/Zr atomic ratio of the powders was 1.136. However, after plasma treatment, the ratio changed into 1.049, which means more Sr than Zr evaporated during plasma treatment of the powders.

During plasma treatment of the powders, the following stages take place: heating of the solid phase, melting of the solid phase, heating of the liquid phase, vaporization, partial or total evaporation and even re-solidification depending on the surrounding temperature and rate of heat transfer (Ref 5, 14). Ceramic particles, especially the ones with low thermal conductivities, start to evaporate after a few millimeters of trajectory, and for ceramics this vaporization starts long before the particle core has begun to melt (Ref 15). During plasma spraying, the temperature of the plasma flame is much higher than the melting point of $SrZrO_3$ and evaporation is inevitable. $SrZrO_3$ decomposes easily at the melting temperature. It can be anticipated that both SrO and ZrO_2 were evaporated during the plasma spray process, the evaporation rate of strontium oxide and zirconia might be quite different by virtue of the differences in their thermophysical properties (like melting point). Table 3 shows a comparison of some thermophysical properties of SrO and ZrO_2, which indicate that the latter is more thermally stable than the former. The evaporation rate is driven by the intrinsic vapor pressure of the material and limited by diffusion of vapor through the boundary layer surrounding the particle surface (Ref 5). Figure 6 indicates vapor pressure of SrO and ZrO_2 at different temperatures. SrO has a higher vapor pressure than ZrO_2, which explains the faster loss of SrO

Table 2 Chemical compositions of the $SrZrO_3$ powders before and after plasma treatment

Powders	Sr, wt.%	Zr, wt.%	Sr/Zr, atomic ratio
Before plasma treatment	40.7	37.3	1.136
After plasma treatment	39.0	38.7	1.049

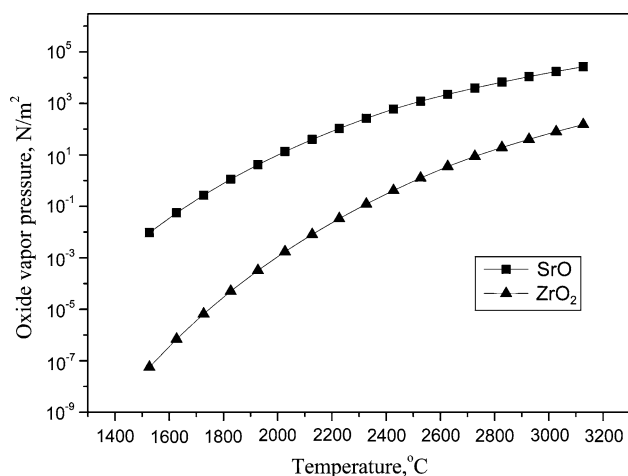**Fig. 6** Oxide vapor pressure of SrO and ZrO$_2$ (Ref 17)

Table 3 Physical properties of SrO and ZrO$_2$ (Ref 16, 17)

Properties	SrO	ZrO$_2$
Melting temperature, K	2804	2963 (β-ZrO$_2$)
Boiling temperature, K	~3273	4573
Heat of sublimation $\Delta H \times 10^{-6}$, J/kg·mole	530.635 ± 12.142	741.064 ± 25.121
Crystal lattice energy, 10^{-6} J/kg·mole	3311.759	11195.503

compared to ZrO$_2$ during plasma spraying. More evaporation of SrO leads to stoichiometry changes. Partial evaporation of SrO also happened when SrZrO$_3$ was synthesized by floating zone technique with radiation heating (Ref 18). An excess of SrCO$_3$ was also added to the feed rod material to compensate the evaporation losses (Ref 18).

The XRD result of spray-dried SrZrO$_3$ powders after plasma treatment is shown in Fig. 7. The main phase composition is still SrZrO$_3$. Traces of SrCO$_3$ (PDF#01-071-2393, Orthorhombic) can be detected.

3.3 Influence of Plasma Spraying Current, Distance and Particle Size on Sr Evaporation

It is well known that spraying parameters can have an important effect on the composition of as-sprayed coatings. Partial evaporation of Sr was found during plasma spraying of SrZrO$_3$ coating. In order to investigate the influence of spraying parameters on the Sr evaporation, parameters including spraying current, distance and particle size were varied. The result is shown in Table 4.

Speed and temperature monitoring of the particles were performed by the particle diagnostic system Accura Spray. Accura Spray is a sensor specifically designed for industrial online monitoring of thermal spray processes. It allows control of coating properties by providing real-time measurements of the average particle temperature, velocity and flow rate as well as the vertical position and
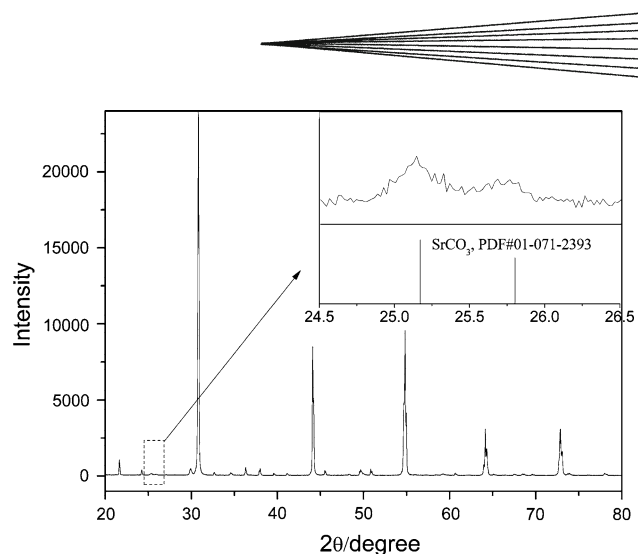

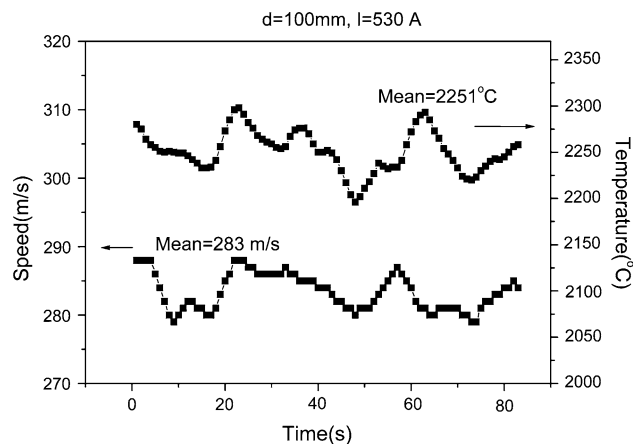**Fig. 7** XRD of spray-dried SrZrO$_3$ powders after plasma treatment

Fig. 8 Speed and temperature of the SrZrO$_3$ particles measured with Accura Spray (plasma current $I = 530$ A, spraying distance $d = 100$ mm)

Table 4 Influences of plasma spraying current, distance and particle size on Sr evaporation

Coating no.	Particle size, μm	Current, A	Spraying distance, mm	Sr/Zr decreased, %
A	45-100	530	200	32.3
B	45-100	440	200	20.2
C	45-100	440	100	19.8
D	45-100	370	200	6.2
E	>100	440	100	13.3
F	>100	370	200	3.8

profile of the plume itself (Ref 19). Particle temperatures are determined by two-color pyrometry and particle velocities are obtained from cross-correlation of signals which are recorded at two closely spaced locations (Ref 20). Figure 8 shows speed and temperature of the SrZrO$_3$ particles measured with Accura Spray (plasma current $I = 530$ A, spraying distance $d = 100$ mm). The measurement time was 80 s. For a current of 530 A, the
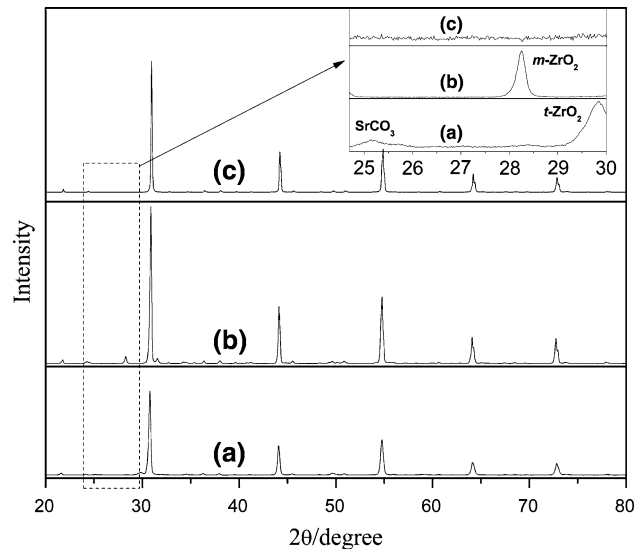
mean particle speed and particle temperature were found to be 283 m/s and 2251 °C, respectively. However, when the current was 370 A, the mean particle speed and particle temperature were reduced to 192 m/s and 1667 °C, respectively. This proves that an increase of spraying current will lead to higher particle temperature and velocity. The heat transfer from the jet to the particles is sufficient to melt more powders and as a result a higher amount of SrO is volatilized. For coatings D, B and A, higher spraying current leads to more Sr evaporation.

The particle size of the powders used for plasma spraying also has an influence on the final Sr/Zr ratio of the coating. The evaporation of SrO can be reduced effectively by increasing the particle size of the powder used for plasma spraying. Comparing with coatings C-D, coatings E-F used larger size powders and showed less Sr evaporation. The rate of heat transfer through the boundary layer is proportional to the surface area of the particle (Ref 14). The evaporation time of a particle is proportional to its surface area and smaller particles have larger evaporation rates (Ref 5, 21). Therefore, the partial evaporation is proportional to the particle diameter. A similar result has also been reported by Cao (Ref 9). During plasma spraying of $La_2Ce_2O_7$, the evaporation of CeO_2 can be reduced effectively by increasing the particle size of the powder for plasma spraying (Ref 9).

For coatings B and C, longer spraying distance leads to a little higher degree of SrO evaporation. With longer spraying distance, the dwell time of the particle in the plume is longer, leading to higher total SrO evaporation.
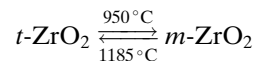
3.4 Stoichiometric SrZrO₃ Coating Received

Figure 9 indicates x-ray diffraction patterns of plasma-sprayed coatings. The main phase for all coatings is $SrZrO_3$ while the secondary phases are different. The peaks at $2\theta = 25.2°, 28.2°, 29.8°$ can be assigned to $SrCO_3$, ZrO_2 (m) and ZrO_2 (t), respectively. Even if coatings were sprayed with different parameters and the resultant Sr/Zr of the as-sprayed coating are different, the phase compositions of all of the as-sprayed coatings indicated by XRD are still the same. The secondary phases of the as-sprayed coatings are $SrCO_3$ and unstable tetragonal ZrO_2 (Fig. 9a). The metastable tetragonal ZrO_2 is typical of thermally sprayed zirconia coatings, which is due to the rapid solidification at a cooling rate >100 K s^{-1} of the melted liquid droplets. Under these conditions, the equilibrium phase was not retained and metastable crystalline or non-crystalline products may be formed (Ref 8). In the near future, thermal cycling test of $SrZrO_3$ coating will be carried out with a surface temperature of 1350 °C. For comparison, these coatings were also sintered at 1350 °C. Thermal treatment can partly regenerate the phase of perovskite. During sintering, all of the newly formed $SrCO_3$ reacted with ZrO_2 (t) to form $SrZrO_3$ again. That is why both of these two peaks disappeared after sintering (Fig. 9b-c). The Sr/Zr ratio has an influence on phase composition of the sintered coating. If Sr/Zr is a little larger than 1, after sintering the phase composition of the coating is pure $SrZrO_3$ (Fig. 9c). Within limits of XRD, no

Fig. 9 (a) $SrZrO_3$ coating in the as-sprayed case; (b) $SrZrO_3$ coating (Sr/Zr = 0.950) after sintered at 1350 °C for 72 h; and (c) coating (Sr/Zr = 1.038) sintered at 1350 °C for 72 h

secondary phases were detected. This means that after sintering, pure $SrZrO_3$ coating can be recovered only when Sr/Zr ratio of the coating is a little larger than 1 (Sr/Zr = 1.038 for this coating). If the Sr/Zr ratio is smaller than 1, m-ZrO_2 can be detected in the coating after sintered at 1350 °C for 72 h (Fig. 9b). During sintering, nonequilibrium t-ZrO_2 transformed into m-ZrO_2 upon cooling according to the following phase transformation:

$$t\text{-}ZrO_2 \underset{1185\,°C}{\overset{950\,°C}{\rightleftharpoons}} m\text{-}ZrO_2$$

3.5 Proposed Forming Mechanisms of Needle-Like Structure and Strontium Carbonate

So far, the detailed forming mechanisms of needle-like structure in powders sprayed into water and $SrCO_3$ in both coatings and powders sprayed into water are still not clear. One mechanism is proposed here.

After spray-drying and before plasma spraying, the powders were annealed at 1300 °C for 5 h to remove organic binder and carbon source. Therefore, the newly formed $SrCO_3$ must have formed during plasma spraying or later. During plasma spraying, molten powders are in contact with the surrounding atmosphere. They may decompose or have chemical reactions with the surrounding atmosphere. For example, oxides might form on the particle surface during plasma spraying of metals. Volatile species might form through thermal decomposition or reaction with the surrounding gas (Ref 5). Like perovskite-structured $LaMnO_3$, $LaCoO_3$ and $YBa_2Cu_3O_x$ (Ref 6, 22), $SrZrO_3$ also decomposes easily at the melting temperature. The needle-like structure is probably formed from completely molten phase originating from the readily

melted ultra-fine Sr-rich $SrZrO_3$ particles in flight. The new structure contained only Sr without Zr. Composition of the needle-like structure may be SrO at the beginning. However, Sr is strong carbonate former like Ba (Ref 23). Formation of $SrCO_3$ from SrO and atmospheric CO_2 for the $SrZrO_3$ coatings or plasma-treated powders might be inevitable.

4. Conclusions

Partial evaporation of SrO happened during plasma spraying of $SrZrO_3$, which is confirmed by plasma spraying of $SrZrO_3$ powders into water. During plasma spraying $SrZrO_3$ into water, some new needle-like structures formed and it contained only Sr. Once the initial composition of the powders is fixed, the final Sr/Zr ratio of the sprayed coating is determined by spraying current, distance and particle size of the powders used. By varying the spraying parameters and adding an excess amount of SrO before plasma spraying, stoichiometric strontium zirconate coatings can be produced. Traces of $SrCO_3$ and metastable tetragonal ZrO_2 can be detected in the as-sprayed coating. During sintering $SrCO_3$ reacts with part of ZrO_2 to form $SrZrO_3$ again and the remaining metastable tetragonal ZrO_2 transformed into ZrO_2 (*m*). After sintering, pure $SrZrO_3$ coating can be received only when the Sr/Zr ratio of the coating is a little larger than 1. In the near future, microstructure optimization and thermal cycling behavior of the received stoichiometric strontium zirconate coating will be investigated.

References

1. R. Vaßen, X. Cao, F. Tietz, D. Basu, and D. Stöver, Zirconates as New Materials for Thermal Barrier Coatings, *J. Am. Ceram. Soc.*, 2000, **83**(8), p 2023-2028
2. W. Ma, D.E. Mack, R. Vaßen, and D. Stöver, Perovskite-Type Strontium Zirconate as a New Material for Thermal Barrier Coatings, *J. Am. Ceram. Soc.*, 2008, **91**(8), p 2630-2635
3. S. Yamanaka, K. Kurosaki, T. Oyama, H. Muta, M. Uno, T. Matsuda, and S. Kobayashi, Thermophysical Properties of Perovskite-Type Strontium Cerate and Zirconate, *J. Am. Ceram. Soc.*, 2005, **88**(6), p 1496-1499
4. Y.C. Lee, Y.P. Chyou, and E. Pfender, Particle Dynamics and Particle Heat and Mass Transfer in Thermal Plasmas. Part II. Particle Heat and Mass Transfer in Thermal Plasmas, *Plasma Chem. Plasma Process.*, 1985, **5**(4), p 391-414
5. Y.P. Wan, J.R. Fincke, S. Sampath, V. Prasad, and H. Herman, Modeling and Experimental Observation of Evaporation from Oxidizing Molybdenum Particles Entrained in a Thermal Plasma Jet, *Int. J. Heat Mass Transf.*, 2002, **45**, p 1007-1015
6. L. Pawlowski, *The Science and Engineering of Thermal Spray Coatings*, Wiley, Chichester, 1995
7. X.Q. Cao, R. Vassen, W. Jungen, S. Schwartz, F. Tietz, and D. Stöver, Thermal Stability of Lanthanum Zirconate Plasma Sprayed Coating, *J. Am. Ceram. Soc.*, 2001, **84**(9), p 2086-2090
8. R. Mcpherson, N. Gane, and T.J. Bastow, Structural Characterization of Plasma sprayed Hydroxylapatite Coatings, *J. Mater. Sci.: Mater. Med.*, 1995, **6**, p 327-334
9. X. Cao, R. Vassen, W. Fischer, F. Tietz, W. Jungen, and D. Stöver, Lanthanum-Cerium Oxide as a Thermal Barrier-Coating Material for High-Temperature Applications, *Adv. Mater.*, 2003, **15**(17), p 1438-1442
10. T. Noguchi, T. Okubo, and O. Yonemochi, Reactions in the System ZrO₂–SrO, *J. Am. Ceram. Soc.*, 1969, **52**(4), p 178-181
11. S. Dyshlovenko, L. Pawlowski, P. Roussel, D. Murano, and A. Le Maguer, Relationship Between Plasma Spray Operational Parameters and Microstructure of Hydroxyapatite Coatings and Powder Particles Sprayed into Water, *Surf. Coat. Technol.*, 2006, **200**, p 3845-3855
12. R.M. Young and E. Pfender, Generation and Behavior of Fine Particles in Thermal Plasmas—A Review, *Plasma Chem. Plasma Process.*, 1985, **5**(1), p 1-37
13. X. Chen and E. Pfender, Unsteady Heating and Radiation Effects of Small Particles in a Thermal Plasma, *Plasma Chem. Plasma Process.*, 1982, **2**(3), p 293-316
14. M. Vardelle, A. Vardelle, K.-I. Li, and P. Fauchais, Coating Generation: Vaporization of Particles in Plasma Spraying and Splat Formation, *Pure Appl. Chem.*, 1996, **68**(5), p 1093-1099
15. M. Vardelle, C. Trassy, A. Vardelle, and P. Fauchais, Experimental Investigation of Powder Vaporization in Thermal Plasma Jets, *Plasma Chem. Plasma Process.*, 1991, **11**(2), p 185-201
16. http://www.hbcpnetbase.com/
17. V. Samsonov, *The Oxide Handbook*, 2nd ed., IFI/Plenum, New York, 1982
18. D. Souptel, G. Behr, and A.M. Balbashov, SrZrO₃ Single Crystal Growth by Floating Zone Technique with Radiation Heating, *J. Cryst. Growth*, 2002, **236**, p 583-588
19. http://www.tecnar.com
20. G. Maurer, R. Vaßen, and D. Stöver, Comparison and Applications of DPV-2000 and Accuraspray-g3 Diagnostic Systems, *J. Therm. Spray Technol.*, 2007, **16**(3), p 414-424
21. X. Chen and E. Pfender, Heat Transfer to a Single Particle Exposed to a Thermal Plasma, *Plasma Chem. Plasma Process.*, 1982, **2**(2), p 185-212
22. C. Monterrubio-Badillo, H. Ageorges, T. Chartier, J.F. Coudert, and P. Fauchais, Preparation of LaMnO₃ Perovskite Thin Films by Suspension Plasma Spraying for SOFC Cathodes, *Surf. Coat. Technol.*, 2006, **200**, p 3743-3756
23. H. Fjellvag, P. Karen, A. Kjekshus, P. Kofstad, and T. Norby, Carbonatization of YBa₂Cu₃O₆₊ₓ, *Acta Chem. Scand. A*, 1988, **42**, p 178-184